

Unconventional singularities and frictional rupture energy budget

Efim A. Brener^{1,2} and Eran Bouchbinder²

¹*Peter Grünberg Institut, Forschungszentrum Jülich, D-52425 Jülich, Germany*

²*Institute for Energy and Climate Research, Forschungszentrum Jülich, D-52425 Jülich, Germany*

³*Chemical and Biological Physics Department, Weizmann Institute of Science, Rehovot 7610001, Israel*

A widespread framework for understanding frictional rupture, such as earthquakes along geological faults, invokes an analogy to ordinary cracks. In ordinary cracks, near rupture edge fields feature a conventional square root singularity, accompanied by an associated edge-localized energy balance. It has been recently demonstrated that this analogy holds to a very good approximation, yet that overall rupture (earthquake) energy budget includes also a significant non-edge-localized excess frictional dissipation, which is predicted to vanish in the crack analogy. We develop a macroscopic theory that address these puzzling observations and fully resolves the apparent contradiction. The theory identifies a “hidden” small parameter, which quantifies the deviation from a conventional singular behavior of near-edge fields, and predicts non-edge-localized excess frictional dissipation that is dominated by an accumulated spatially-extended contribution. The latter, which is also position dependent, is associated with the generic rate-dependent nature of friction and compensates the aforementioned smallness. The theoretical predictions are quantitatively supported by available numerical results, and their possible implications for earthquake physics are discussed.

The failure of frictional systems, composed of bodies interacting along contact interfaces, is mediated by the propagation of interfacial frictional rupture [1–3]. A prominent example for such spatiotemporal frictional rupture processes is earthquakes along geological faults [3–7]. A widespread framework for understanding frictional rupture invokes a close analogy to ordinary cracks [8–23], despite notable differences in the underlying physics. Most importantly, an ordinary crack leaves behind it fully-broken, stress-free surfaces, while the interface left behind a frictional rupture front remains in contact and hence features a finite frictional stress (strength) τ . Moreover, not only τ does not vanish as in ordinary cracks, but in fact it is a dynamical field that varies in space and time, and that depends on the local slip rate/velocity v and on the instantaneous structural state of the frictional interface.

The rather well-developed theory of ordinary cracks, the so-called Linear Elastic Fracture Mechanics (LEFM) [24, 25], offers powerful tools that would be very useful for understanding, interpreting and quantifying frictional rupture, if the analogy holds. LEFM is based on scale separation between edge-localized dissipation, which takes place on a short lengthscale ℓ , and linear elastic driving energy, which is stored on significantly larger scales. In particular, cracks in the LEFM framework are characterized by edge-localized energy dissipation per unit area G_c (the so-called fracture energy), which is balanced by an elastic energy flux G into the edge region, and by near-edge singular fields that are characterized by a universal $-\frac{1}{2}$ exponent [24, 25].

Recently, it has been shown that generic rate-and-state dependent frictional dynamics give rise to frictional rupture that appears to closely resemble ordinary

cracks [22, 23], see Fig. 1. In particular, it has been shown that the frictional stress τ behind frictional rupture approaches a constant residual value τ_{res} [22, 23] (a corresponding residual slip velocity v_{res} is also approached, see Fig. 1); once the dynamics are quantified relative to the residual stress, frictional rupture has been shown to be characterized by a well-defined edge-localized dissipation G_c (an effective fracture energy), featuring a localization length ℓ (cf. Fig. 1), and by near-edge fields that follow the conventional LEFM $-\frac{1}{2}$ singularity to a very good approximation [23]. Furthermore, the singular field are associated with an elastic energy flux G that approximately balances G_c , $G \approx G_c$, which in turn determines the rupture velocity c_r [23].

Yet, the very same analysis gave rise to a set of puzzling observations [23], suggesting that there remain fundamental open questions regarding the analogy between frictional rupture and ordinary cracks. To describe these puzzling observations, consider two symmetrically propagating frictional rupture fronts (under 2D anti-plane conditions [23]) that nucleated at $x = 0$ (the hypocenter, cf. Fig. 1) at time $t = 0$. The frictional interface follows a generic rate-and-state constitutive relation [26–33], characterized by an N -shaped steady-state friction curve $\tau_{\text{ss}}(v)$ [34, 35] and a single structural state field $\phi(x, t)$ [26–38], as detailed in [22, 23] and in the Materials and Methods. For a broad range of materials, $\tau_{\text{ss}}(v)$ is characterized by a non-monotonic and rather weak logarithmic rate-dependence [35]. The instantaneous position of each rupture front is $L(t)$ (we focus hereafter on the right-propagating one) and its instantaneous velocity is $c_r(t) = \dot{L}(t)$, cf. Fig. 1. Consider then a fixed position x_i away from the hypocenter and track there the frictional stress $\tau(t; x_i)$ and the slip displace-

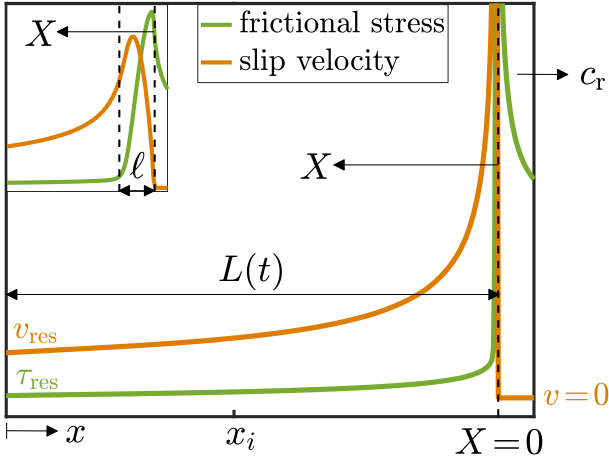


FIG. 1. A frictional rupture front that nucleated at $x = 0$ and propagates to the right in a 2D anti-plane rate-and-state friction simulation (its symmetric counterpart, propagating to the left, is shown in Fig. 3a of [23], see details about the computer simulation therein). Its instantaneous half-length is $L(t)$ and instantaneous propagation velocity is $c_r(t) \simeq 0.94c_s$. Shown are the frictional stress (strength) field $\tau(X, t)$ (green) and slip velocity field $v(X, t)$ (orange) left behind the propagating edge. Here $X(t)$ is a coordinate moving with the edge and pointing backwards, whose origin ($X(t) = 0$) is defined according to $v = 0$. The two fields approach finite residual values, τ_{res} and v_{res} , respectively, far behind the propagating edge. (inset) A zoom in on the edge region, revealing a localization lengthscale ℓ associated with edge-localized dissipation, resulting in an effective fracture energy G_c (see [23], and also Fig. 2, for a precise definition of ℓ). $v(x, t)$ follows, to a very good approximation, the conventional square root singularity of LEFM at an intermediate region, i.e. $X > \ell$ and prior to approaching v_{res} (fit not shown here, see [23]). The same conventional singularity is featured by $\tau(X, t)$ ahead of the edge, $X < 0$ and $|X| > \ell$, but it is not discussed here [23].

ment $\delta(t; x_i) = \int_{t_{x_i}}^t v(t; x_i) dt$, where t_{x_i} is defined such that $L(t_{x_i}) = x_i$.

In order to address and quantify the energy budget associated with frictional rupture propagation — i.e. “earthquake” energy budget — we consider the breakdown energy at the observation point x_i , defined as $E_{\text{BD}}(t; x_i) = \int_0^{\delta(t; x_i)} [\tau(\delta'; x_i) - \tau_{\text{res}}] d\delta'$ [39]. The term “breakdown” refers here to the fact that E_{BD} involves stresses surpassing τ_{res} , i.e. it does not account for the background frictional dissipation (heat) associated with sliding against the residual stress. For ordinary cracks, $E_{\text{BD}}(t; x_i)$ is predicted to be independent of x_i and to increase over a short timescale $\ell/c_r(t_{x_i})$ (for $t > t_{x_i}$), until it saturates at G_c . In light of the very good agreement between frictional rupture and ordinary cracks in terms of the near-edge singularity and edge-localized energy balance, we expect $E_{\text{BD}}(t; x_i)$ of frictional rupture to follow these predictions. In Fig. 2, we present $E_{\text{BD}}(t; x_i)$ for 4 different observation points x_{1-4} along the fault/interface (data adapted from Fig. 3a in [23]).

Here we parameterize $E_{\text{BD}}(t; x_i)$ according to the distance $X(t) \equiv L(t) - x_i$ between the observation point and the rupture edge (cf. Fig. 1), instead of using t itself.

It is observed that $E_{\text{BD}}(X(t); x_i)$ increases up to G_c on a short timescale corresponding to the near-edge localization length ℓ , and that it does so independently of x_i , as expected for ordinary cracks. Yet, in sharp contrast to the ordinary cracks predictions, the 4 curves do not saturate at $E_{\text{BD}}(X(t); x_i) = G_c$, but rather they branch out, keep on increasing and appear to saturate at x_i -dependent values that are substantially larger than G_c . How is it possible that frictional rupture features the conventional square root singularity and the edge-localized energy balance $G = G_c$ to a very good approximation, and at the same time $E_{\text{BD}}(X(t); x_i)$ significantly exceeds the edge-localized dissipation G_c ? What is the origin of the x_i dependence of $E_{\text{BD}}(X(t); x_i)$? What physics controls the x_i -dependent saturation level? In this work, we develop a comprehensive theory that fully and quantitatively resolves these puzzles, revealing fundamental properties of frictional rupture with possible implications for earthquake physics.

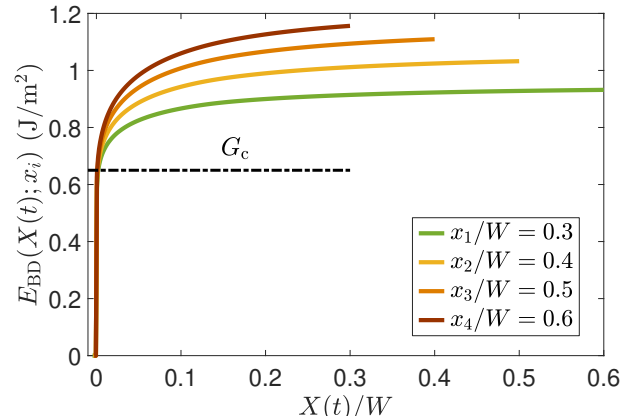


FIG. 2. The breakdown energy $E_{\text{BD}}(t; x_i) = \int_0^{\delta(t; x_i)} [\tau(\delta'; x_i) - \tau_{\text{res}}] d\delta'$, here parameterized by $X(t) \equiv L(t) - x_i$ (cf. Fig. 1), as a function of $X(t)/W$ for $t > t_{x_i}$ (see text for definition). It is calculated for 4 different observation points x_{1-4} (see legend) in the simulation whose results are shown in Fig. 1. W is the fault/interface half-length and we set $t_{x_i} = 0$ for $i = 1-4$ (for presentational convenience). All curves perfectly overlap over a short lengthscale, which identifies with ℓ (see Fig. 1 and [23]), defining the effective fracture energy G_c (dashed-dotted horizontal line), but branch out on larger scales. See text for additional discussion.

THEORY OF THE BREAKDOWN ENERGY

In order to develop a theory of frictional rupture energy budget, one needs to calculate the dimensionless excess breakdown energy, defined as $\Delta E_{\text{BD}}(X; x_i) \equiv (E_{\text{BD}}(X; x_i) - G_c)/G_c$, where the term “excess” refers

here to the dissipation on top of the effective fracture energy G_c . To that aim, consider a frictional rupture front steadily propagating at a constant velocity c_r , for which the slip displacement increment at any point on the fault/interface takes the form $d\delta = v(X; c_r, L) dX/c_r$. With this relation at hand, one can use the definition of E_{BD} to define $\Delta\mathcal{E}_{BD}^T$ through the following spatial integral

$$\Delta\mathcal{E}_{BD}^T(X; c_r, L, \ell) = (1)$$

$$(G_c c_r)^{-1} \int_\ell^X [\tau(X'; c_r, L) - \tau_{\text{res}}] v(X'; c_r, L) dX' ,$$

for $\ell \leq X \leq L$ (cf. Fig. 1, where ℓ , X and L are illustrated), where we used the fact that the integral over $0 \leq X < \ell$ equals G_c .

The superscript T, standing for “Theory”, highlights the fact that $\Delta\mathcal{E}_{BD}^T(X; c_r, L, \ell)$ cannot be immediately identified with $\Delta\mathcal{E}_{BD}(X; x_i)$; the former is a spatial integral over a snapshot of the rupture fields that makes no explicit reference to an observation point x_i , it explicitly involves the rupture size L and it is strictly valid for steady-state propagation conditions. The latter is defined at an observation point x_i , it makes no reference to the rupture size L and it is valid for non-steady propagation conditions (in fact, the results presented in Fig. 2 correspond to a continuously accelerating rupture, $\dot{c}_r(t) > 0$, cf. [23] and below). The relations between $\Delta\mathcal{E}_{BD}^T(X; c_r, L, \ell)$ and $\Delta\mathcal{E}_{BD}(X; x_i)$ will be discussed in detail below, but one should first calculate the former.

The starting point for our development is the observation that $[\tau(X; c_r, L) - \tau_{\text{res}}]/\tau_{\text{res}} \ll 1$ for $X > \ell$ (cf. Fig. 1). Had it been $\tau(X > \ell; c_r, L) = \tau_{\text{res}}$, we would have $\Delta\mathcal{E}_{BD} = 0$ and the conventional slip velocity singularity $v(X; c_r, L) \sim 1/\sqrt{X}$ would have been exact for $\ell \ll X \ll L$. Therefore, we treat the latter as a leading order solution and aim at expressing $\tau(X; c_r, L) - \tau_{\text{res}}$ in terms of $v(X; c_r, L)$. We then assume that the evolution of the internal state field $\phi(X, t)$ is “fast”, i.e. that it quickly equilibrates with $v(X; c_r, L)$. Under these conditions, we are left with $\tau(X; c_r, L) = \tau_{\text{ss}}[v(X; c_r, L)]$, where the latter is a nonlinear relation. To allow for an analytic treatment, we further assume that the smallness of $(\tau_{\text{ss}}(v) - \tau_{\text{res}})/\tau_{\text{res}}$ also implies the smallness of $(v - v_{\text{res}})/v_{\text{res}}$, presumably justifying a linearization of $\tau_{\text{ss}}(v) - \tau_{\text{res}}$ around $v = v_{\text{res}}$ for the entire range $X > \ell$.

With these ideas and assumptions in mind, we obtain the following expansion

$$\tau_{\text{ss}}(v) - \tau_{\text{res}} \simeq (d\tau_{\text{ss}}(v_{\text{res}})/dv)(v - v_{\text{res}}) \approx \eta v , \quad (2)$$

where $\eta \equiv d\tau_{\text{ss}}(v_{\text{res}})/dv$ and $\tau_{\text{res}} \gg v_{\text{res}} d\tau_{\text{ss}}(v_{\text{res}})/dv$ is typically satisfied. As will be shown next, this effective linear viscous-friction relation allows to gain deep analytical insight into the physics of the problem at hand [40]. Plugging Eq. 2 into Eq. 1, we obtain $\Delta\mathcal{E}_{BD}^T(X; c_r, L, \ell) = \frac{\eta}{G_c c_r} \int_\ell^X [v(X'; c_r, L)]^2 dX'$. Using then the conventional singular slip velocity field

$v(X; c_r, L) \simeq 2c_r K / [\mu \alpha_s(c_r) \sqrt{2\pi X}]$ for anti-plane conditions [24, 25], where $\alpha_s(c_r) = \sqrt{1 - c_r^2/c_s^2}$ is the relativistic Lorentz factor and K is the stress intensity factor, we can perform the integration to obtain

$$\Delta\mathcal{E}_{BD}^T(X; c_r, L, \ell) \simeq \Delta\xi(c_r) \ln(X/\ell) , \quad (3)$$

which is expected to hold for $\ell \ll X \ll L$, and where

$$\Delta\xi(c_r) \equiv \frac{4\eta c_r}{\pi \mu \alpha_s(c_r)} . \quad (4)$$

In deriving Eq. 3, we used the edge-localized energy balance $G = K^2 / [2\mu \alpha_s(c_r)] = G_c$ [24, 25], which is associated with dissipation on the scale $X \sim \ell$.

The effective viscous-friction coefficient η is positive for the N-shaped steady-state friction curve $\tau_{\text{ss}}(v)$ because v_{res} typically resides on the velocity-strengthening branch of the friction law above its minimum, $d\tau_{\text{ss}}(v_{\text{res}})/dv > 0$. While there is ample evidence that the N-shaped steady-state curve is a generic property of frictional interfaces [35], hence $\eta > 0$, it is important to note that having $\eta = d\tau_{\text{ss}}(v_{\text{res}})/dv < 0$ does not violate any law of nature. The point is that $\Delta\mathcal{E}_{BD} \times G_c$ is not the total dissipation, which includes also G_c , the background frictional dissipation associated with sliding against the residual stress τ_{res} and radiated energy. Together, these ensure positive total dissipation and in principle one can have $\eta < 0$, which implies $\Delta\mathcal{E}_{BD} < 0$. This would be the case if v_{res} resides on a velocity-weakening branch of the friction curve, $d\tau_{\text{ss}}(v_{\text{res}})/dv < 0$.

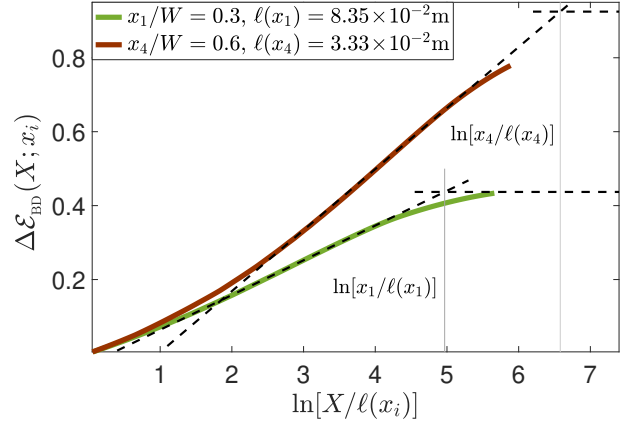


FIG. 3. $\Delta\mathcal{E}_{BD}(X; x_i)$, presented in Fig. 2, vs. $\ln[X/\ell(x_i)]$ for $x_1/W = 0.3$ and $x_4/W = 0.6$ (see legend). $\Delta\mathcal{E}_{BD}(X; x_i)$ follows a logarithmic behavior at an intermediate range, as highlighted by the titled dashed lines (the slope of the lower line is 0.094 and that of the upper one is 0.165, their ratio is 1.76). $\Delta\mathcal{E}_{BD}(X; x_i)$ presumably crosses over, roughly at $\ln[x_i/\ell(x_i)]$ (light gray vertical lines), to a plateau (illustrated by the horizontal dashed lines).

COMPARISON TO NUMERICAL SIMULATIONS

Equations 3-4 constitute a major result of this work. To understand their physical content and implications, note first that Eq. 3 predicts that $\Delta\mathcal{E}_{\text{BD}}^{\text{T}}$ varies predominantly logarithmically with X in the intermediate range $\ell \ll X \ll L$. This analytic prediction is directly tested in Fig. 3, where $\Delta\mathcal{E}_{\text{BD}}$ of Fig. 2 is replotted (for the lowest and largest x_i 's) against $\ln(X/\ell)$. It is observed, as predicted, that $\Delta\mathcal{E}_{\text{BD}}$ for the two extreme values of x_i depends logarithmically on X in an intermediate range. The slope/prefactor of the logarithmic law depends on the observation point x_i , where in the examples presented the one for x_4 is 1.76 times larger than that of x_1 (which is closer to the hypocenter). Equation 4 predicts that the prefactor of the logarithmic dependence in Eq. 3 may depend on x_i only through $c_r(t)$, and in particular through the combination $c_r/\alpha_s(c_r)$ (assuming the effective linear viscous-friction coefficient η is the same for the two curves). Indeed, as mentioned above, frictional rupture in this numerical simulation continuously accelerated, where we have $c_r(t_{x_1})=0.94c_s$ and $c_r(t_{x_4})=0.983c_s$. Using these, we obtain a slopes ratio of 1.94, in reasonably good quantitative agreement with the 1.76 observation.

With these encouraging results at hand, we are ready to resolve the main puzzle posed in this work. We first evaluate $\Delta\xi(c_r)$ in Eq. 4 for the simulational results presented in Figs. 1-2, obtaining $\Delta\xi(c_r) \sim \mathcal{O}(10^{-1})$, which is in the right ballpark compared to the prefactors of the logarithmic law observed in Fig. 3. $\Delta\mathcal{E}_{\text{BD}}$ can be, and in fact is, quite significantly larger than $\Delta\xi(c_r)$ due to accumulated spatial contribution associated with the huge difference between X (that can reach the fault/interface size) and the localization length ℓ (and despite the logarithmic dependence on their ratio). We thus conclude that the non-edge-localized excess breakdown energy in Eq. 3 is a product of a typically small number, given by Eq. 4, and an accumulated spatially-extended contribution that can compensate the smallness of $\Delta\xi(c_r)$.

RELATION TO UNCONVENTIONAL SINGULARITIES

How then can a significant non-edge-localized excess breakdown energy $\Delta\mathcal{E}_{\text{BD}}$ exist, hand in hand with a good agreement with the conventional square root singularity, which requires edge-localized dissipation? The key to answer this question is $\Delta\xi(c_r)$ and its physical meaning. While it is common to assume that the conventional square root singularity of LEFM remains valid for frictional rupture, and while this assumption is a posteriori supported by some observations, for the effective linear viscous-friction in Eq. 2 nothing should be assumed, the singularity order can be explicitly derived (due to the

linearity of the problem). That is,

$$v(X; c_r) \sim (X/\ell)^{\xi(c_r)}, \quad (5)$$

where $\xi(c_r)$ does not necessarily and a priori equal $-\frac{1}{2}$, i.e. it may correspond to an *unconventional singularity* emerging from the intrinsic rate-dependence of the frictional stress [40].

Using Eq. 2 and specializing here for anti-plane conditions, one can show that $\xi(c_r)$ satisfies $\cot[\pi\xi(c_r)] = -2\eta c_r/[\mu\alpha_s(c_r)]$ (see Materials and Methods). This relation shows that the singularity order is not a constant, but rather a dynamic quantity that varies with the rupture velocity c_r . Moreover, assuming that $\xi(c_r)$ indeed deviates from $-\frac{1}{2}$ only slightly, we obtain

$$\xi(c_r) \simeq -\frac{1}{2}[1 - \Delta\xi(c_r)], \quad (6)$$

where surprisingly $\Delta\xi(c_r)$ is *the same* one given in Eq. 4, which has already been shown to be quite significantly smaller than unity. Equation 6, together with Eqs. 3-4, provide a complete and physically transparent solution to the major problem posed in this work.

Equation 6 shows that frictional rupture is in fact characterized by an unconventional singularity, yet that the deviation from the conventional $-\frac{1}{2}$ singularity is small due to the smallness of $\Delta\xi$, demonstrated above. The excess breakdown energy $\Delta\mathcal{E}_{\text{BD}}$ in Eq. 3 is proportional to the very same small quantity $\Delta\xi$, given in Eq. 4, but $\Delta\mathcal{E}_{\text{BD}}$ is not necessarily small because the smallness of $\Delta\xi$ may be compensated by an accumulated spatially-extended contribution. Therefore, we identify $\Delta\xi$ as *hidden small parameter* in frictional failure dynamics. The origin of this small parameter is the rate-dependence of the frictional stress, which in turn implies that the strict scale separation assumed in LEFM is only approximately valid in frictional rupture dynamics (manifested in the slow decay of $\tau(X)$ toward τ_{res}). Moreover, some physical quantities (e.g. $\Delta\mathcal{E}_{\text{BD}}$) may be more strongly affected than others (e.g. ξ) by the lack of strict scale separation. Finally, we note that for other interfacial constitutive relations $\Delta\xi$ may not be small and additional new physics may emerge. Such situations will not be extensively discussed here, but will be mentioned below in relation to seismological observations.

THE POSITION DEPENDENCE OF THE BREAKDOWN ENERGY AND ADDITIONAL COMPARISON TO NUMERICAL SIMULATIONS

The main assumption behind the theory developed so far was that $\tau_{\text{ss}}(v) - \tau_{\text{res}}$ can be linearized around v_{res} . While plausible, the smallness of $(\tau_{\text{ss}}(v) - \tau_{\text{res}})/\tau_{\text{res}}$ does not strictly guarantee that the linear relation in Eq. 2 is quantitatively accurate over the entire range $X > \ell$, which involves a rather broad range of slip velocities (e.g. linearization around a different v could lead

to more accurate quantitative predictions). In addition, the analysis up to now focussed on the singular part of $v(X; c_r, L)$, which cannot remain valid for sufficiently large X 's. The larger X 's behavior is also intimately related to the remaining open questions concerning the x_i -dependent saturation of $\Delta\mathcal{E}_{\text{BD}}$. To address these issues, we reevaluate the integral in Eq. 1 using the fully nonlinear N -shaped $\tau_{\text{ss}}(v)$ (see Materials and Methods); in addition, for $v(X; c_r, L)$ we use Broberg's full-field solution for a self-similar crack propagating at a constant velocity c_r . The latter, which includes higher order contributions on top of the singular one, takes the form $v(X; c_r, L) = c_r \sqrt{\frac{8 G_c L}{\pi \mu \alpha_s(c_r)}} / \sqrt{L^2 - (L - X)^2}$ [25], and is valid for $\ell \leq X \leq L$.

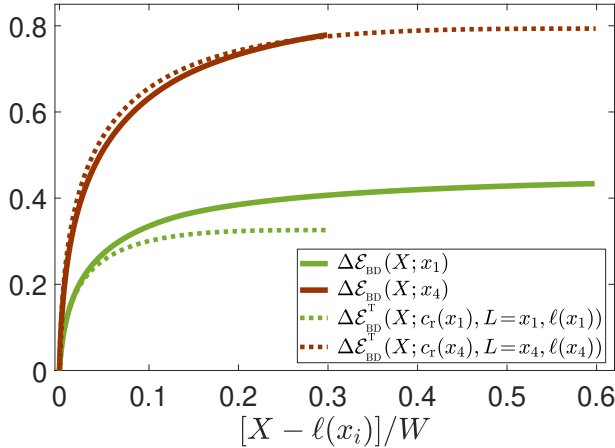


FIG. 4. The simulational $\Delta\mathcal{E}_{\text{BD}}(X; x_i)$ (solid lines, see legend), presented in Fig. 2, and the theoretical $\Delta\mathcal{E}_{\text{BD}}^T(X; c_r(x_i), L = x_i, \ell(x_i))$ (dashed lines, see legend) of Eq. 1 (see text for additional details), vs. $[X - \ell(x_i)]/W$ for $x_1/W = 0.3$ and $x_4/W = 0.6$ (see legend). The values of $\ell(x_i)$ are given in Fig. 3. Note that the theoretical curves, by construction, extend up to $X = x_i$ (recall that $\ell(x_i) \ll x_i$) and that the simulational ones are limited by the fault/interface half-length W , the smaller x_i the larger the maximal X .

It is important to note that both the just-described procedure and the one developed previously are perturbation theories based on the LEFM solution as the leading order contribution, used to calculate the relevant dissipation integral in the main approximation [40]. In the first procedure, $\tau_{\text{ss}}(v) - \tau_{\text{res}}$ is linearized around v_{res} and only the singular part of $v(X)$ is considered, while in the second one, no linearization of the interfacial constitutive relation is performed and the relevant full-field LEFM solution is used. The former integral was evaluated analytically, leading to deep insights, while the latter inevitably involves numerical integration.

Before performing the numerical integration, we also note that it has been established above that the singular part of $v(X)$ gives rise to the logarithmic dependence $\ln(X/\ell)$, which was discussed and validated in the in-

termediate range $\ell \ll X \ll L$. This behavior, however, cannot persist indefinitely; when does it break down? does $\Delta\mathcal{E}_{\text{BD}}$ actually saturate after the $\ln(X/\ell)$ law breaks down or does it diverge with increasing L and X ? Answering these questions will allow us to address the x_i -dependent saturation of $E_{\text{BD}}(X; x_i)$, observed in Fig. 2 (additional x_i dependence, manifested in the prefactor of the $\ln(X/\ell)$ law, has been associated with the non-steady nature of rupture propagation, cf. Fig. 2).

To address these questions, note that during crack propagation, the relation $L(t) = x_i + X(t)$ holds for $L(t) \geq x_i$, where both $L(t)$ and $X(t)$ increase, while x_i is fixed. At short propagation times, measured relative to the time at which $L(t) = x_i$, we have $X \ll x_i$. At intermediate propagation times, $\Delta\mathcal{E}_{\text{BD}}(X; x_i)$ varies logarithmically with X , as demonstrated in Fig. 3, and finally, at long propagation times, we have $X(t) \rightarrow L(t)$, which implies $X \gg x_i$ and for which the logarithmic law is not valid anymore. If for large X $\tau_{\text{ss}}[v(X; c_r, L)]$ approaches τ_{res} in a way that leads to the *saturation* of $\Delta\mathcal{E}_{\text{BD}}(X)$, then we expect the logarithmic behavior of $\Delta\mathcal{E}_{\text{BD}}(X; x_i)$ to cross over to a plateau on a scale $X \sim x_i$, i.e. when $\ln(X/\ell)$ roughly equals $\ln(x_i/\ell(x_i))$. This prediction is tested and supported in Fig. 3, demonstrating that $\Delta\mathcal{E}_{\text{BD}}(X; x_i)$ indeed crosses over to a plateau on a scale $X \sim x_i$.

This insight allows us to relate the theoretical $\Delta\mathcal{E}_{\text{BD}}^T(X; c_r, L, \ell)$ of Eq. 1, which is a spatial integral over a snapshot of the rupture fields that in itself is independent of the observation point x_i , to the observation point dependence of $\Delta\mathcal{E}_{\text{BD}}(X; x_i)$. In particular, as the integral in Eq. 1 extends up to $X = L$, the saturation at $X \sim x_i$ can be captured by setting $L = x_i$. It is important to note that this saturation is totally unrelated to the additional x_i dependence introduced by the non-steadiness of rupture propagation. The latter, as already discussed earlier, is captured by setting $c_r = c_r(x_i)$ and $\ell = \ell(x_i)$. Consequently, we calculated $\Delta\mathcal{E}_{\text{BD}}^T(X; c_r(x_i), L = x_i, \ell(x_i))$ of Eq. 1 using the fully nonlinear N -shaped $\tau_{\text{ss}}(v)$ (see Materials and Methods) and Broberg's full-field solution $v(X; c_r(x_i), L = x_i)$, and compared it to $\Delta\mathcal{E}_{\text{BD}}(X; x_i)$ in Fig. 4. The comparison reveals reasonable quantitative agreement between the theory and the simulation, lending strong support to former.

POSSIBLE IMPLICATIONS FOR SEISMOLOGICAL OBSERVATIONS

As explained above, the breakdown energy constitutes an important contribution to the total frictional rupture energy budget, which includes also the background frictional dissipation (heat) and the radiated energy. In the context of earthquake physics, these three contributions sum up to the potential energy release during an earthquake [10]. It would be interesting to discuss whether,

and if so to what extent, our theory might have some implications for seismological observations. The latter typically aim at using source spectra to obtain coarse-grained average estimates of the following quantity [9, 12, 41–44]

$$G_f(\delta) \equiv \int_0^\delta [\tau(\delta') - \tau(\delta)] d\delta'. \quad (7)$$

Note that $G_f(\delta)$ differs from the breakdown energy $E_{BD}(\delta; x_i) = \int_0^\delta [\tau(\delta'; x_i) - \tau_{res}] d\delta'$ in two respects. First, it makes no reference to a fault observation point x_i . Second, the reference stress used in it is $\tau(\delta)$, rather than the constant residual stress τ_{res} .

Before discussing seismological observations, let us calculate $G_f(\delta)$ in the framework of the theory developed in this work. As explained above, the dissipation in the spatial range $0 \leq X \leq \ell$ near the rupture edge gives rise to a well-defined effective fracture energy G_c , marked in Fig. 2. The edge-localized dissipation G_c is related to a strong strength reduction (cf. Fig. 1) over a characteristic slip displacement δ_c , such that $G_f(\delta_c) = G_c$ (note that G_c of Fig. 2, which is based on E_{BD} , slightly differs in its value from the one associated with G_f due to the difference in the definition of these quantities). This strong frictional strength reduction is associated in the rate-and-state constitutive framework with the evolution of the internal state field ϕ . It has been shown [45, 46] that while the rate-and-state constitutive framework does not make explicit reference to δ , the strength reduction from τ_0 — reached after the very initial increase in slip velocity near the rupture edge — to τ_c at $\delta = \delta_c$ (where τ_c is close to, but still larger than, τ_{res}) follows an effective linear slip-weakening law of the form $\tau(\delta) \simeq \tau_0 - (\tau_0 - \tau_c)\delta/\delta_c$. Plugging the latter into Eq. 7, we obtain

$$G_f(\delta) \sim \delta^2 \quad \text{for} \quad \delta \leq \delta_c. \quad (8)$$

According to Eq. 8, $G_f(\delta)$ follows a quadratic power law for $\delta \leq \delta_c$, i.e. for $G_f(\delta) \leq G_c$. For $\delta > \delta_c$, where the frictional strength slowly reduces from τ_c to the residual stress τ_{res} (cf. Fig. 1, τ_c is not marked), $G_f(\delta)$ is associated with the dissipation in the extended spatial range $X > \ell$. Our viscous-friction theory predicts that the excess dissipation in this range — on top of G_c — is intimately related to the emergence of unconventional singularities in frictional rupture, which in turn mainly depend on the rate-dependence of friction (and not on the internal state field ϕ). To obtain $G_f(\delta)$ in this regime, we use the slip velocity in Eq. 5, the viscous-friction relation in Eq. 2 and the steady-state relation $v = c_r d\delta/dX$. These yield $\tau(\delta) - \tau_{res} \sim \delta^{\frac{1}{1+\xi}}$, which upon substitution inside Eq. 7 leads to

$$G_f(\delta) - G_c \sim \delta^{\frac{1+2\xi}{1+\xi}} \quad \text{for} \quad \delta > \delta_c. \quad (9)$$

For the conventional singularity, $\xi = -\frac{1}{2}$, Eq. 9 predicts that G_f is independent of δ for $\delta > \delta_c$, as expected (in

fact, the pre-factor also vanishes in this case, implying $G_f = G_c$). In cases in which unconventional singularities emerge, Eq. 9 predicts a power law that depends on the unconventional singularity order ξ .

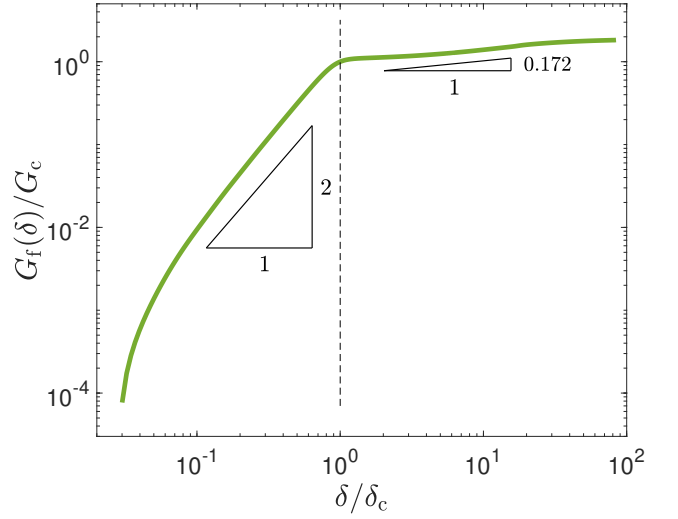


FIG. 5. $G_f(\delta)$, defined in Eq. 7, for the very same rupture simulation whose results are presented in Figs. 2–4 (for the observation point $x_1/W = 0.3$). $G_f(\delta)$ features two power laws, marked by the two triangles, in agreement with the theoretical predictions in Eqs. 8–9. The crossover between the two power laws, marked by the vertical dashed line, occurs at (δ_c, G_c) , as predicted theoretically. G_c and δ_c are used to normalize G_f and δ , respectively (the value used for the former, $G_c = 0.51 \text{ J/m}^2$, is slightly smaller than the one observed in Fig. 2 due to the difference in the definition of G_f and E_{BD}). Finally, comparing the power law exponent in the $\delta > \delta_c$ regime, 0.172, to the analytic prediction in Eq. 9 and using the transformation $\xi = -\frac{1}{2}(1 - \Delta\xi)$ (cf. Eq. 6), one obtains $\Delta\xi = 0.094$. The latter is in perfect quantitative agreement with $\Delta\xi$ extracted in Fig. 2 (see also Eqs. 3–4).

Our theory thus predicts that $G_f(\delta)$ follows a quadratic power law for $\delta \leq \delta_c$, cf. Eq. 8, which is associated with the strong frictional strength reduction taking place near the rupture edge. The quadratic law is a signature of an effective linear slip-weakening characterizing this strength reduction process. At $G_f(\delta_c) = G_c$, the theory predicts a crossover to another power law, valid for $\delta > \delta_c$ (cf. Eq. 9), which is associated with spatially-extended dissipation and is determined by the unconventional singularity order ξ . These predictions are being tested in Fig. 5 for the smallest x_i data presented earlier in Figs. 2–4 (green curves). The numerical results quantitatively agree with the theoretical predictions, revealing a quadratic power law at small δ as predicted by Eq. 8, and a weaker power law (here with an exponent 0.172) for $G_f(\delta) > G_c$, as predicted by Eq. 9. Using the latter, together with the transformation $\xi = -\frac{1}{2}(1 - \Delta\xi)$ (cf. Eq. 6), one obtains $\Delta\xi = 0.094$, which is in perfect quantitative agreement with $\Delta\xi$ extracted in Fig. 2 (see also Eqs. 3–4).

Note that $\Delta\xi$ exhibits some dependence on the observation point x_i (cf. Fig. 2), which is not discussed here since seismological observations — to be considered next — completely lack the spatial resolution required to reveal this dependence.

As explained above, seismological observations aim at using source spectra to obtain coarse-grained average estimates of G_f in Eq. 7, e.g., see [12, 41–44]. Yet, such seismological observations completely lack the spatiotemporal resolution to probe the slip δ as a function of time at a given observation point x_i on the fault. Instead, it is common to plot the seismological estimate of G_f as a function of the total average slip $\bar{\delta}$ in an earthquake, making no explicit reference to the spatiotemporal evolution of slip during rupture. Moreover, it is common to superimpose the seismological estimates of G_f vs. $\bar{\delta}$ for many earthquakes (including both crack-like and pulse-like events) occurring on different faults in a single plot, while it is not a priori clear that the data should at all collapse on a master curve. Finally, natural faults exhibit richer constitutive behaviors at high slip velocities (e.g. related to flash weakening and thermal pressurization [42]) compared to the rate-and-state framework used in this work, feature geometrical complexity and are 3D in nature. Yet, with these caveats in mind and following other authors [12, 41–43], we identify $\bar{\delta}$ with δ and discuss the *qualitative salient features* of the theoretical predictions in Eqs. 8–9 in relation to the available G_f vs. $\bar{\delta}$ seismological observations.

Various authors compiled seismological observations from many earthquakes on different faults, spanning a broad range of total average slip $\bar{\delta}$, ranging from the micron scale to the scale of tens of meters [12, 41–43]. Several authors [41, 42] reported $G_f(\bar{\delta}) \sim \bar{\delta}^2$ for relatively small $\bar{\delta}$, consistently with Eq. 8, i.e. with an effective linear slip-weakening behavior near the rupture edge. Others, e.g. [12, 43], suggested a weaker-than-quadratic small $\bar{\delta}$ power law and interpreted it in terms of a sub-linear slip-weakening behavior near the rupture edge. None of these, to the best of our knowledge, managed to single out G_c — i.e. the part of G_f that is balanced the edge-localized energy flux G and that in turn controls the rupture propagation velocity — from the data, as our theory allows.

Probably most relevant for our theoretical predictions are the data compiled in [42], where a quadratic power law $G_f(\bar{\delta}) \sim \bar{\delta}^2$ at small $\bar{\delta}$ appears to cross over to a weaker power law $G_f(\bar{\delta}) \sim \bar{\delta}^{2/3}$ at large $\bar{\delta}$. This behavior appears to be in *qualitative* agreement with the theoretical predictions in Eqs. 8–9, suggesting that different physics controls the two power law regimes, and in particular that the latter is associated with an unconventional singularity and a dissipation contribution from a spatially-extended region behind the rupture edge. Interestingly, the two power laws suggested in [42] have been interpreted in terms of a thermal pressurization constitutive

model, where the fluid pore pressure plays a central role. The quadratic power law has been interpreted to correspond to an effective linear slip-weakening behavior associated with undrained conditions and the 2/3 power law with drained conditions [42]. Most interestingly, the 2/3 power law regime has been related to an unconventional singularity of order $\xi = -\frac{1}{4}$, associated with the thermal pressurization model under drained conditions and corresponding to large slips accumulated far behind the rupture edge. In fact, substituting $\xi = -\frac{1}{4}$ in Eq. 9, one obtains a 2/3 power law, even though the linear viscous-friction approximation of Eq. 2 does not seem to be directly relevant to the analysis of [42].

CONCLUSION

In this work we developed a theory that explains how, and under what conditions, frictional rupture can feature the conventional LEFM near-edge singularity and energy balance to a very good approximation, and at the same time a non-edge-localized breakdown energy that significantly deviates from the edge-localized dissipation. As such, the theory sheds basic light on frictional rupture energy budget and the underlying lengthscales. The crux of the theory is the identification of a hidden small parameter $\Delta\xi$ that quantifies the deviation from the conventional LEFM singularity and that is intrinsically related to the rate dependence of friction, $d\tau_{ss}(v)/dv \neq 0$. The theory quantitatively explains recent puzzling observations in cutting-edge numerical simulations and offers predictions that are amenable to laboratory testing using available techniques [1]. Finally, the theory offers tools and concepts that can be used to interpret seismological estimates of earthquake breakdown energies.

Methods — This work is analytic in nature and all of the derivations are detailed in the text, except for the solution for the unconventional singularity order, which is provided below. The theoretical predictions are compared to numerical results that have been published in [23] based on 2D anti-plane spectral boundary integral method simulations [47–49]. These numerical simulations employed a rate-and-state friction constitutive relation $\tau = \sigma \operatorname{sgn}(v) f(|v|, \phi)$, where σ is the normal stress and $f(|v|, \phi) = [1 + b \log(1 + \phi/\phi_*)][f_0/\sqrt{1 + (v_*/v)^2} + a \log(1 + |v|/v_*)]$. The internal state field ϕ satisfies $\dot{\phi} = 1 - \sqrt{1 + (v_*/v)^2} |v| \phi / D$ and the values of the parameters appear in Table I in [22]. Under steady-state conditions, $\phi = 0$, the frictional strength $\tau_{ss}(v)$ follows an N -shaped curve, as plotted in Fig. 2a of [22] and in Fig. 1b of [23], and as supported by numerous experiments [35]. The numerical results of [23] have been presented in this work in different forms, depending on the theoretical predictions being tested, as detailed in the

text.

The unconventional singularity order ξ can be obtained by considering the interfacial boundary condition for 2D anti-plane steadily propagating rupture [50]

$$\tau(X) = \frac{\mu \alpha_s(c_r)}{2\pi c_r} \int_0^\infty \frac{v(X')}{X' - X} dX' , \quad (10)$$

where the left-hand-side is the frictional strength and the right-hand-side is the shear stress at the interface, as obtained from bulk elastodynamics [50]. Using $\tau_{ss}(v)$ of Eq. 2 for $\tau(X)$ and invoking the asymptotic power law ansatz in Eq. 5, Eq. 10 implies that the unconventional singularity order ξ satisfies $\cot(\pi \xi) = -2 \eta c_r / (\mu \alpha_s(c_r))$, as reported in the text. Finally, plugging into the last relation Eq. 6 and expanding to the leading order in $\Delta \xi$, the latter is calculated and is shown to identify with Eq. 4, as stated in the text.

Acknowledgements — We are grateful to F. Barras for critically reading the manuscript, for pushing us to think about seismological observations, and for his help with Figs. 1, 2 and 5. We thank T. Roch for his help with Figs. 1-2 and Y. Lubomirsky for his help with the numerical integration in relation to Fig. 4. E.B. acknowledges support from the Israel Science Foundation (Grants No. 295/16 and 1085/20), the Ben May Center for Chemical Theory and Computation, and the Harold Perlman Family.

[1] Svetlizky I, Bayart E, Fineberg J (2019) Brittle Fracture Theory Describes the Onset of Frictional Motion. *Annu. Rev. Condens. Matter Phys.* 10(1):031218–013327.

[2] Ben-Zion Y (2001) Dynamic ruptures in recent models of earthquake faults. *J. Mech. Phys. Solids* 49(9):2209–2244.

[3] Scholz CH (2002) *The mechanics of earthquakes and faulting*. (Cambridge university press).

[4] Rice JR (1980) The mechanics of earthquake rupture in *Phys. Earth's Inter.* pp. 555–649.

[5] Kostrov B, Das S (1988) *Principles of earthquake source mechanics*. (Cambridge University Press), p. 286.

[6] Kanamori H, Brodsky EE (2004) The physics of earthquakes. *Reports Prog. Phys.* 67(8):1429–1496.

[7] Ohnaka M (2013) *The physics of rock failure and earthquakes*. (Cambridge University Press).

[8] Ida Y (1972) Cohesive force across the tip of a longitudinal-shear crack and Griffith's specific surface energy. *J. Geophys. Res.* 77(20):3796–3805.

[9] Palmer AC, Rice JR (1973) The Growth of Slip Surfaces in the Progressive Failure of Over-Consolidated Clay. *Proc. R. Soc. A Math. Phys. Eng. Sci.* 332(1591):527–548.

[10] Kanamori H, Heaton TH (2000) Microscopic and macroscopic physics of earthquakes in *Geocomplexity Phys. Earthquakes*. (American Geophysical Union (AGU)), pp. 147–163.

[11] Das S (2003) Dynamic fracture mechanics in the study of the earthquake rupturing process: theory and observation. *J. Mech. Phys. Solids* 51(11-12):1939–1955.

[12] Abercrombie RE, Rice JR (2005) Can observations of earthquake scaling constrain slip weakening? *Geophys. J. Int.* 162(2):406–424.

[13] Lu X, Rosakis AJ, Lapusta N (2010) Rupture modes in laboratory earthquakes: Effect of fault prestress and nucleation conditions. *J. Geophys. Res. Solid Earth* 115(12):1–25.

[14] Lu X, Lapusta N, Rosakis AJ (2010) Pulse-like and crack-like dynamic shear ruptures on frictional interfaces: experimental evidence, numerical modeling, and implications. *Int. J. Fract.* 163(1-2):27–39.

[15] Noda H, Lapusta N, Kanamori H (2013) Comparison of average stress drop measures for ruptures with heterogeneous stress change and implications for earthquake physics. *Geophys. J. Int.* 193(3):1691–1712.

[16] Svetlizky I, Fineberg J (2014) Classical shear cracks drive the onset of dry frictional motion. *Nature* 509(7499):205–208.

[17] Kammer DS, Radiguet M, Ampuero JP, Molinari JF (2015) Linear Elastic Fracture Mechanics Predicts the Propagation Distance of Frictional Slip. *Tribol. Lett.* 57(3):23.

[18] Svetlizky I, et al. (2016) Properties of the shear stress peak radiated ahead of rapidly accelerating rupture fronts that mediate frictional slip. *Proc. Natl. Acad. Sci.* 113(3):542–547.

[19] Bizzarri A, Liu C (2016) Near-field radiated wave field may help to understand the style of the supershear transition of dynamic ruptures. *Phys. Earth Planet. Inter.* 261:133–140.

[20] Rubino V, Rosakis AJ, Lapusta N (2017) Understanding dynamic friction through spontaneously evolving laboratory earthquakes. *Nat. Commun.* 8(7260):15991.

[21] Svetlizky I, Bayart E, Cohen G, Fineberg J (2017) Frictional Resistance within the Wake of Frictional Rupture Fronts. *Phys. Rev. Lett.* 118(23):234301.

[22] Barras F, et al. (2019) The emergence of crack-like behavior of frictional rupture: The origin of stress drops.

[23] Barras F, et al. (2020) The emergence of crack-like behavior of frictional rupture: Edge singularity and energy balance. *Earth and Planetary Science Letters* 531:115978.

[24] Freund LB (1998) *Dynamic Fracture Mechanics*. (Cambridge university press, Cambridge).

[25] Broberg KB (1999) *Cracks and fracture*. (Academic Press).

[26] Dieterich JH (1979) Modeling of rock friction: 1. experimental results and constitutive equations. *Journal of Geophysical Research: Solid Earth* 84(B5):2161–2168.

[27] Ruina AL (1983) Slip instability and state variable friction laws. *J. Geophys. Res.* 88(B12):10359–10370.

[28] Rice JR, Ruina AL (1983) Stability of Steady Frictional Slipping. *J. Appl. Mech.* 50(2):343–349.

[29] Dieterich JH (1994) A constitutive law for rate of earthquake production and its application to earthquake clustering. *J. Geophys. Res. Solid Earth* 99(B2):2601–2618.

[30] Marone C (1998) The effect of loading rate on static friction and the rate of fault healing during the earthquake cycle. *Nature* 391(6662):69–72.

[31] Nakatani M (2001) Conceptual and physical clarification of rate and state friction: Frictional sliding as a thermally activated rheology. *J. Geophys. Res. Solid Earth*

106(B7):13347–13380.

[32] Rice JR, Lapusta N, Ranjith K (2001) Rate and state dependent friction and the stability of sliding between elastically deformable solids. *J. Mech. Phys. Solids* 49(9):1865–1898.

[33] Baumberger T, Caroli C (2006) Solid friction from stick-slip down to pinning and aging. *Adv. Phys.* 55(3-4):279–348.

[34] Bar Sinai Y, Brener EA, Bouchbinder E (2012) Slow rupture of frictional interfaces. *Geophys. Res. Lett.* 39(3):L03308.

[35] Bar-Sinai Y, Spatschek R, Brener EA, Bouchbinder E (2014) On the velocity-strengthening behavior of dry friction. *J. Geophys. Res. Solid Earth* 119(3):1738–1748.

[36] Dieterich JH (2007) Applications of rate-and state-dependent friction to models of fault slip and earthquake occurrence. *Treatise Geophys.* 4:107–129.

[37] Nagata K, Nakatani M, Yoshida S (2012) A revised rate- and state-dependent friction law obtained by constraining constitutive and evolution laws separately with laboratory data. *J. Geophys. Res. Solid Earth* 117(B2):B02314.

[38] Bhattacharya P, Rubin AM (2014) Frictional response to velocity steps and 1-D fault nucleation under a state evolution law with stressing-rate dependence. *J. Geophys. Res. Solid Earth* 119(3):2272–2304.

[39] Bizzarri A (2010) On the relations between fracture energy and physical observables in dynamic earthquake models. *J. Geophys. Res.* 115(B10):B10307.

[40] Brener EA, Marchenko VI (2002) Frictional shear cracks. *J. Exp. Theor. Phys. Lett.* 76(4):211–214.

[41] Tinti E, Spudich P, Cocco M (2005) Earthquake fracture energy inferred from kinematic rupture models on extended faults. *J. Geophys. Res.* 110(B12):B12303.

[42] Viesca RC, Garagash DI (2015) Ubiquitous weakening of faults due to thermal pressurization. *Nat. Geosci.* 8(11):875–879.

[43] Nielsen SB, et al. (2016) Scaling in natural and laboratory earthquakes. *Geophys. Res. Lett.* 43(4):1504–1510.

[44] Brantut N, Viesca RC (2017) The fracture energy of ruptures driven by flash heating. *Geophys. Res. Lett.* 44(13):6718–6725.

[45] Cocco M, Bizzarri A (2002) On the slip-weakening behavior of rate- and state dependent constitutive laws. *Geophys. Res. Lett.* 29(11):1516.

[46] Bizzarri A, Cocco M (2003) Slip-weakening behavior during the propagation of dynamic ruptures obeying rate- and state-dependent friction laws. *J. Geophys. Res.* 108(B8):2373.

[47] Geubelle P, Rice JR (1995) A spectral method for three-dimensional elastodynamic fracture problems. *J. Mech. Phys. Solids* 43(11):1791–1824.

[48] Morrissey JW, Geubelle PH (1997) A numerical scheme for mode III dynamic fracture problems. *Int. J. Numer. Methods Eng.* 40(7):1181–1196.

[49] Breitenfeld MS, Geubelle PH (1998) Numerical analysis of dynamic debonding under 2D in-plane and 3D loading. *Int. J. Fract.* 93(1/4):13–38.

[50] Weertman J (1980) Unstable slippage across a fault that separates elastic media of different elastic constants. *J. Geophys. Res. Solid Earth* 85(B3):1455–1461.